Research Paper

EARTHQUAKE SPECTRA

Earthquake Spectra
2023, Vol. 39(2) 727–747

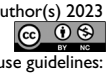

DOI: 10.1177/87552930231152512
journals.sagepub.com/home/eqs

Seismic loss and resilience assessment of tall-coupled cross-laminated timber wall building

Tian You, S.M.EERI[1,2,3], Biniam Tekle Teweldebrhan, S.M.EERI[3], Wei Wang[1,2], and Solomon Tesfamariam, M.EERI[3]

Abstract

Balloon-type cross-laminated timber coupled-wall (CLT-CW) structure is an emerging and sustainable option for constructing tall timber buildings. The structure features buckling restrained brace (BRB) hold-downs, balloon-type CLT walls, and coupling beams with replaceable shear links. This study investigates the probabilistic seismic performance (including economic loss, downtime, and resilience index) of a 20-story CLT-CW building. A three-dimensional (3D) structural model is developed to perform incremental dynamic analysis using 30 pairs of ground motion records that represent the seismicity of Vancouver, Canada. Intensity- and time-based loss assessments are conducted to estimate probability distributions of seismic losses according to the FEMA P-58 methodology. Post-earthquake recovery trajectories of the housing function are also presented to calculate the seismic resilience indices under different intensities. The results reveal that the coupling beams contribute the most to repair cost among all structural components. In light of the replaceability and energy dissipating role of coupling beams, the efficiency and resiliency of the CLT-CW building are validated.

Keywords

Cross-laminated timber (CLT), replaceable shear links, coupling beam, FEMA P-58, probabilistic loss assessment, seismic resilience

Date received: 16 May 2022; accepted: 3 January 2023

[1]State Key Laboratory of Disaster Reduction in Civil Engineering, Tongji University, Shanghai, China
[2]Department of Structural Engineering, Tongji University, Shanghai, China
[3]School of Engineering, The University of British Columbia, Kelowna, BC, Canada

Corresponding author:
Solomon Tesfamariam, School of Engineering, The University of British Columbia, Okanagan Campus, 3333 University Way, Kelowna, BC V1V1V7, Canada.
Email: solomon.tesfamariam@ubc.ca

Introduction

With increase in greenhouse gas emissions, global resource consumption and energy use, there is a demand for cost-effective and sustainable construction materials (Harte, 2017; Svatoš-Ražnjević et al., 2022). In the move toward sustainable construction, timber and timber-based products are becoming viable solutions (Harte, 2017; Milaj et al., 2017). Recent technical advancements in engineered timber products (e.g. glue-laminated timber (GLT), cross-laminated timber (CLT), nail-laminated timber) enabled timber-based construction to be the primary building material in low- to mid-rise residential buildings (Karacabeyli and Gagnon, 2019; Svatoš-Ražnjević et al., 2022). The 2020 National Building Code of Canada (NBC, 2020) and the 2021 International Building Code (Breneman and Richardson, 2019) have increased the mass-timber building heights to 12 and 18 stories, respectively. Tesfamariam et al. (2021a), and Teweldebrhan and Tesfamariam (2022) have recently proposed and designed novel 20-story CLT coupled-wall (CLT-CW) building system. With increase in building height, the need to assess the continuous operation of the system and reduce economic losses under strong earthquake ground shaking becomes a critical design consideration (Di Cesare et al., 2020; Tesfamariam, 2022; Wilson et al., 2021). Thus, in this article, the seismic loss (in terms of monetary repair cost and downtime) and resilience (i.e. the capacity of function recovery in post-event phase) of the 20-story CLT-CW building system reported in literature (Tesfamariam et al., 2021a; Teweldebrhan and Tesfamariam, 2022) are computed. Performance- and resilience-based seismic designs are two philosophies that appropriately address this need.

Prescriptive seismic design aims at preventing collapse and loss of life, but is insufficient to realize a resilient community (Bruneau and MacRae, 2017). After 2011 Christchurch earthquake, for example, a number of buildings in Central Business District area were demolished due to high repair costs although most did not collapse. On the contrary, performance-based earthquake engineering (PBEE) framework emphasizes the importance of loss assessment, which provides results more understandable to clients and stakeholders (Gunay and Mosalam, 2013; Mitrani-Reiser, 2007; Moehle and Deierlein, 2004). Accordingly, based on the early research by the Pacific Earthquake Engineering Research (PEER) Center, a comprehensive state-of-the-art methodology has been formulated to assess the economic losses, downtime, and casualties due to earthquake damage of buildings (FEMA 2006, 2018). Correlated engineering demand parameters (EDPs) can be simulated by assuming multivariate lognormal distribution, and based on the component fragility database, damage states and other consequences of structural and nonstructural components can be derived. The resilience-based evaluation and design is gaining traction in the field of earthquake engineering (Bruneau et al., 2003; Cimellaro et al., 2010). The seismic resilience of a building is its ability to absorb earthquake effects and restore its function (e.g. housing, healthcare, business) to the pre-earthquake normal state. It provides a quantitative measure that considers not only the initial losses right after earthquakes but also the post-earthquake function recovery process. Some research explored the ways of incorporating PBEE into the framework of resilience assessment (Almufti and Willford, 2013; Burton et al., 2016, 2018; Cook et al., 2022; Mieler et al., 2015).

With the increase in popularity of timber-based construction, limited studies are reported on seismic loss and resilience of mass timber buildings. Using the FEMA P-58 methodology, Guan et al. (2018) evaluated the earthquake-induced economic losses of six-story self-centering and welded moment-resisting frames. Pei et al. (2017, 2018, 2019) presented development and validation of a seismic design philosophy for resilient tall wood

buildings. Wilson et al. (2021) implemented the loss assessment for two (5- and 12-story) prototype post-tensioned CLT buildings using the FEMA P-58 procedure. Integrating the FEMA P-58 methodology and REDi™ rating system, Furley et al. (2021) assessed the downtime of a two-story mass timber building. Medel-Vera and Contreras (2021) proposed a seismic resilience-based model to predict economic and environmental losses, and used the tool to assess a six-story CLT building equipped with base isolation devices.

Using the FEMA P-58 procedure, this study presents intensity- and time-based loss assessments to estimate seismic loss and resilience of a 20-story CLT-CW system reported in literature (Tesfamariam et al., 2021a; Teweldebrhan and Tesfamariam, 2022). The system examined in this article was designed considering a coupling ratio (*CR*) of 30% and seismic modification factor (R_oR_d) of 3. *CR* value measures the part of base moment converted into wall axial forces by means of shear forces developed in the coupling beams. Three-dimensional (3D) model of the system is modeled in OpenSees and is subjected to 30 ground motion (GM) records (bi-directional) that were selected to represent the seismicity of Vancouver, Canada. Incremental dynamic analyses (IDAs) are performed and the collapse fragility is derived. After performing intensity-based loss assessment, the probability distributions of seismic losses are presented per level of spectral accelerations. A seismic hazard curve (SHC) is incorporated to estimate mean annual losses (MALs). Post-earthquake recovery of housing functionality of the building is quantified through calculating functional downtime, and seismic resilience is quantified following the well-known dimensionless resilience index (Bruneau et al., 2003; Cimellaro et al., 2010). The rest of this document is organized in six sections. The section "Building model and design details" introduces the building model and design details followed by the section "Numerical model and GM selection" that discusses the OpenSees numerical model of the system and the selected GM records. The sections "Performance assessment" and "Seismic loss assessment" present the seismic loss and resilience assessment of the proposed system. Finally, the section "Conclusion" provides the concluding remarks.

Building model and design details

Building model

Layouts of the CLT-CW building are shown in Figure 1. The structural model comprises glulam beams and columns, CLT floor panels, CLT core shear walls, BRB hold-downs, and steel coupling beams with replaceable shear links. Timber species Spruce–Pine–Fir and Douglas–Fir–Larch are used for the CLT (wall and floor) panels and glulam frame elements, respectively. The glulam beams and columns are designed to support the vertical gravity load of the system, while the balloon CLT shear walls and coupling beams resist the lateral loads. The balloon shear-wall system, which consists of continuous walls over the entire height of the building with the intermediate floor panels framed to the walls at each floor, is chosen over the platform-type construction to prevent the buildup of compression on the floor panels (Chen and Popovski, 2020; Shahnewaz et al., 2021). In the proposed system, the CLT floor panels are supported by the glulam frame elements (beams and columns) and, when applicable, by the CLT shear walls (Structurlam, 2021). The height of the first story is 3.2 m, while the height of the rest stories is 2.96 m. The maximum spans between the gravity columns are 7.315 and 7.204 m in the X- and Y-directions, respectively. The complete architectural drawing of the system with all the dimensions is provided in the study by Tesfamariam et al. (2021a). The apartment building is designed considering four load cases: dead load (D), live load due to use and occupancy

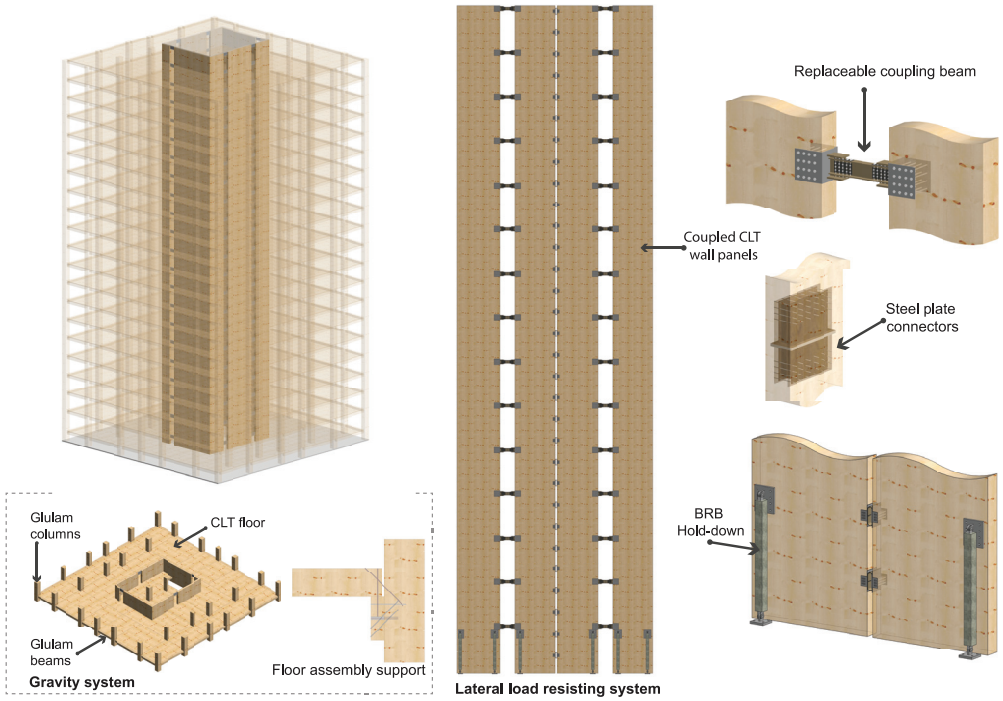

Figure 1. 3D view and structural components of the prototype model.

(L), load due to snow and rain (S), and earthquake load (E). The maximum load obtained from the combination of the above-mentioned load cases was used to design the members. As per the NBC (2020), the building is designed with an $L = 2.4$ kPa and a superimposed load $= 2.8$ kPa to account for the weight of floor finishes and partition load. The prototype building is located in Vancouver—British Columbia (BC), and the corresponding snow and seismic loads are determined based on the provisions of NBC (2020). The CLT floor panels are designed as a one-way slab using a five-ply CLT Grade E1 per ANSI/APA PRG 320 (2012) and CSA 086-19 (2019). The force parameters for the gravity load design of the GLT columns, beams, and CLT wall piers are then extracted from ETABS analysis of the structure and are designed following the CSA 086-19 (2019) standard. The reason why the grade E1 CLT panels are chosen is because the spacing between the columns and the column to the shear walls is large, and there is a high flexural demand in the floor panel.

Seismic design

The seismic design of the CLT-CW system is carried out using continuous medium method (CMM; Smith and Coull, 1991). The method is a simplified elastic method that can be used to analyze and design the preliminary geometries of CW systems for a uniform or quasi-uniform structure. The design, using the simplified method, provides a good approximation for preliminary designs of regular CW systems and should be accompanied by a more accurate nonlinear analysis method to evaluate the system's performance. Accordingly, in this article, the CMM and FEM are used to design the parameters of the lateral load resisting

Table 1. Designed section details

No.	Structural elements	Designed section	Remark
1	CLT roof and floor panels	5-ply (175 mm)	
2	CLT shear walls	9-ply (315 mm)	X-direction (2W system)
3	CLT shear walls	7-ply (245 mm)	Y-direction (3W system)
4	Glulam beams	215 mm × 342 mm	All beams
5	Glulam columns	365 mm × 1064 mm	All columns
6	Coupling beam yield strength (kN)	232	X-direction (2W system)
7	Coupling beam yield strength (kN)	101	Y-direction (3W system)
8	Hold-down yield strength (kN)	2698 and 8465	X-direction (2W system)
9	Hold-down yield strength (kN)	1659 and 4990	Y-direction (3W system)

CLT: cross-laminated timber; W: wall.

system and to study the nonlinear responses of the structure under the action of different GM records, respectively. The summary designed cross-section of the different structural components of the proposed system is summarized in Table 1. The complete design procedure for a two-wall system, along with a numerical example, is provided in the studies by Tesfamariam et al. (2021a), and Teweldebrhan and Tesfamariam (2022).

Numerical model and GM selection

Numerical model

A finite element (FE) model for a 3D CLT-CW building was developed using Open System for Earthquake Engineering Simulation (OpenSees; McKenna et al., 2000). The model is formed by assembling the model components: CLT shear-wall elements, GLT frame elements, hold-downs, and coupling beams. All the timber elements are modeled as elastic. The connections between the CLT to coupling beams and CLT to hold-downs are modeled as rigid connections. The CLT wall panel possesses high elastic stiffness, and it essentially behaves as a rigid body during in-plane response. Consequently, the CLT wall panels are modeled as elastic using *ElasticIsotropic* material and *quad* elements (Demirci et al., 2018). GLT frame elements (beams and columns) are modeled using the OpenSees *elasticBeamColumn* element feature. The two ends and central "fuse" of the coupling beams are modeled using OpenSees *elasticBeamColumn elements as rigid offsets and Steel01 UniaxialMaterial* with *zeroLength* nonlinear vertical springs, respectively. To satisfy the high axial demand, BRB hold-down (Tesfamariam et al., 2021b) is modeled using OpenSees *Steel01 uniaxialMaterial*. The contact between the CLT wall and the base is modeled using OpenSees *uniaxial elastic notension* (ENT) material. A large elastic stiffness value is assigned to the *ENT* spring under compression. However, fracture or deterioration of hold-downs or coupling beams is not explicitly modeled. Damage levels of these components are determined from peak axial strain and peak link rotation angles. The CLT floor panels are assumed as rigid diaphragms and simplified OpenSees' multi-point constraints feature is used to capture the desired behavior without compromising the actual phenomenon (Fairhurst et al., 2014). The detail modeling and modeling parameter values can be obtained in the study by Tesfamariam et al. (2021a).

GM selection

The building was design for the seismicity of Vancouver, BC—Canada. GM records are selected by matching the response spectra of the selected records to a target response

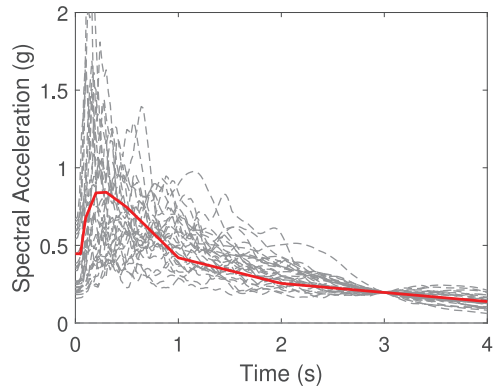

Figure 2. Spectral acceleration (in *g*) at 3.0 s. for Vancouver, BC—Canada.

spectrum of Vancouver with a return period of 2475 years. In this study, conditional mean spectrum (CMS) is used to define the target response spectrum (Baker, 2011). Three major seismic sources (crustal, inslab, and interface) contribute most significantly to the overall seismic hazard of Vancouver (Goda and Atkinson, 2011; Halchuk et al., 2016). Accordingly, multiple-CMS-based record selection method is used to select a suite of GM records that possess key features (e.g. magnitude, frequency content, and duration) of the considered seismic sources (Goda and Atkinson, 2011). The number of GM records selected from each source reflects the proportion of their seismic hazard contribution. Same selection method has been successfully implemented to develop the seismic fragility curves of different limit states for buildings (Tesfamariam et al., 2021b; Tesfamariam and Goda 2015, 2022). Their analyses were based on a two-dimensional FE model, while a 3D model is developed in this study for the proposed system. As a result, the coupled GM selected were used for bi-directional input. As part of the GM selection process, it is important to determine the first three fundamental periods of a structure. In this study, an eigen analysis was performed and the first three fundamental periods of the building were found to be 2.87, 1.52, and 0.57 s. Hence, a set of 30 GM records (bi-directional) were selected based on regional seismic hazard characteristics at the anchor period of $T_A = 3.0$ s, corresponding to the return period of 2475 years. Moreover, vibration periods of $T_{min} = 0.1$ s and $T_{max} = 4.0$ s were considered as the lower and upper limit for the GM selection. Figure 2 shows the 5%-damped spectral accelerations of the selected GM records. The same 30 GMs will be scaled to a series of intensities under which seismic loss and resilience are assessed.

Performance assessment

Time history responses

The nonlinear time history analysis (NLTHA) at the 2475-year return period intensity is used to assess the nonlinear response of the systems under the action of seismic excitation. It is found that the CLT-CW system exhibits higher responses (e.g. inter-story drifts, floor accelerations, and shear forces of coupling beams) in the weakest (X) direction, and the results for this direction are discussed below. Figure 3 illustrates the inter-story drift ratio (ISDR), floor acceleration time series, and coupling beam response for GM (#30) in the X-direction. For the examined system, there are a total of 40 coupling beams (2 coupling

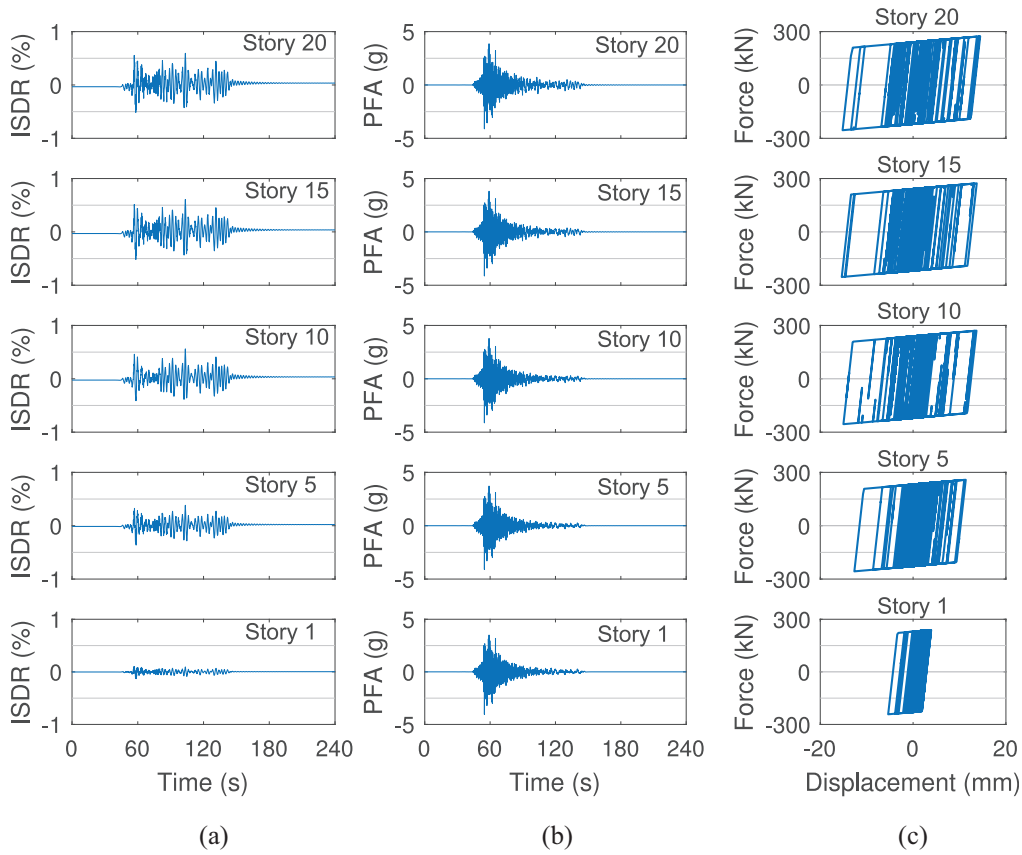

Figure 3. Time-history responses: (a) ISDR, (b) floor acceleration, and (c) coupling beam response for GM #30 along the X-direction.

beams at each story level) in the X-direction (two-wall system) and 80 coupling beams (4 coupling beams at each story level) in the Y-direction (three-wall system). Accordingly, the shear force demand of coupling beams in the X-direction is higher than the coupling beams in the Y-direction. As a result, the coupling beams in the X-direction have a higher strength and lower response in contrast to those in the Y-direction that have lower strength and higher responses. In both directions, uniform coupling beam capacity is provided throughout the height of the building (Figure 3c) and thus, coupling beams at higher stories experience a higher drift demand (due to cantilever action of the wall) and exhibit higher hysteresis responses than those in the lower stories. Moreover, Figures 4 and 5 show the response of the BRB hold-downs, provided at the base of the CLT shear walls, in the X- and Y-directions at selected GM records. In Figure 4, HD_{3X} and HD_{4X} represent the BRB hold-downs for the larger CLT wall (and vice versa). Similar HD_{3Y} and HD_{4Y} in Figure 5 represent the BRB hold-downs for the larger (middle) CLT wall. Same capacity hold-downs were provided at the left and right base of each CLT wall panel. As the hold-downs at the outer sides of the CLT walls are subjected to higher axial action than those located at the inner sides, higher displacement is observed in the outer hold-downs. For the same GM, the coupling beam displacement is higher than the hold-down's displacement, which satisfies the requirements of same CSA O86-19 (2019) and Canadian CLT

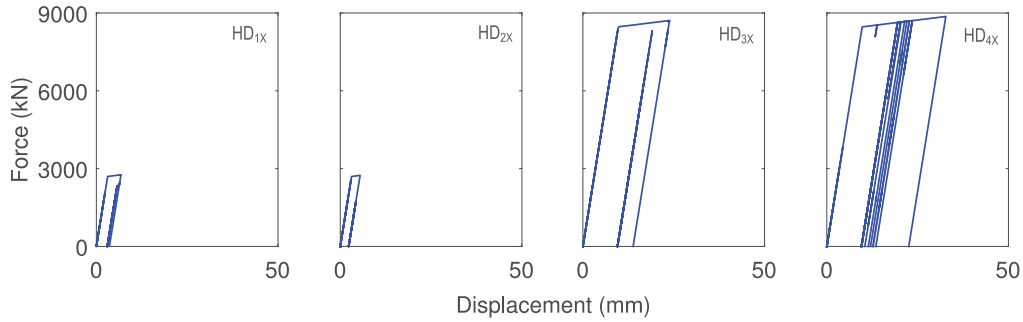

Figure 4. Hold-down response for GM #30 along the X-direction.

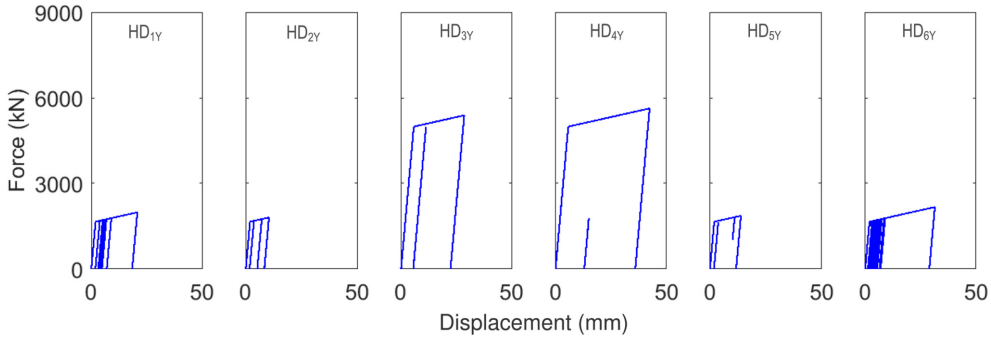

Figure 5. Hold-down response for GM #30 along the Y-direction.

handbook (2019) that requires discrete hold-downs to yield after the primary energy-dissipating elements (e.g. vertical shear connections, shear links) and slightly contribute to energy dissipation.

Incremental dynamic analysis

IDA is performed to examine the performance of the CLT-CW system under the action of different seismic hazard levels. The GM records are scaled up until a spectral acceleration value that triggered the collapse of the system (MaxISDR = 5%). The typical IDA curves for the CLT-CW system (in the X- and Y-directions) are shown in Figure 6a and b, respectively. The horizontal and vertical axes represent the MaxISDR and 5% spectral acceleration at the fundamental period of the system ($S_a(T_1)$), respectively. In CW systems and CLT connection design, yielding is preferred to occur at the primary energy dissipation system followed by the yielding of the secondary energy dissipation system (SCB shear links and hold-downs in this system, respectively). For a CLT-CW system, it is shown that all the coupling beams yield before the yielding of the hold-downs (Teweldebrhan and Tesfamariam, 2022). Under modest levels of earthquakes, the system behaves elastically. However, as the GM intensity increases, the coupling beams start to yield and the coupling action degrades. Furthermore, the slope of the IDA falls as the hold-downs start to yield and the curve flattens out to indicate that the systems have suffered significant drift damage before reaching the collapse points.

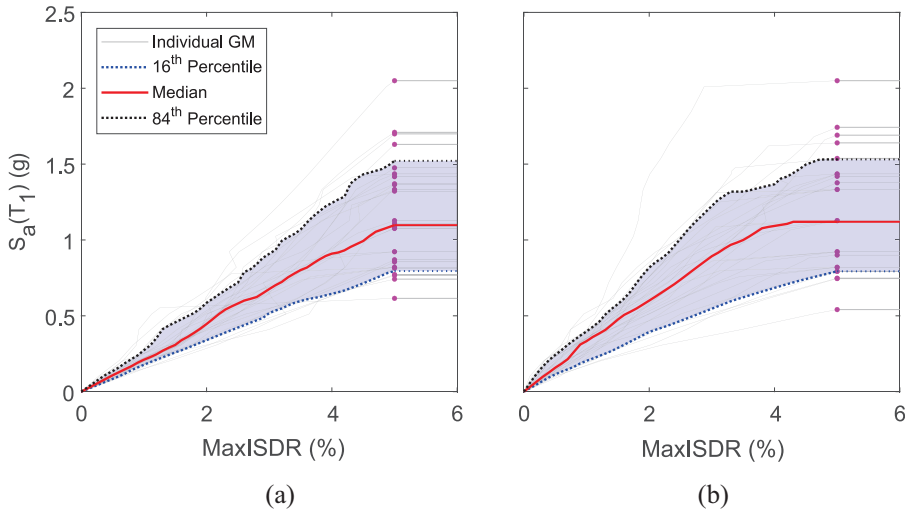

Figure 6. IDA curves along (a) X- and (b) Y-directions.

Seismic loss assessment

Methodology of probabilistic seismic loss assessment

The methodology in FEMA P-58 (2018) is applied to perform probabilistic seismic loss assessment of the CLT-CW building. Intensity- and time-based loss assessments are conducted in turn. An intensity-based assessment is to estimate the probability distribution of seismic losses under a certain seismic intensity. In a time-based assessment, losses from different intensities are combined into MALs based on their probability of occurrence. The spectral acceleration at the building fundamental period is selected as the intensity measure herein. The examined target intensities range from 0.05 to 0.6*g*, to consider the seismic losses incurred by different levels of intensities.

An intensity-based assessment consists of five steps, as shown in Figure 7. (1) A set of GM records (the same 30 records as in the previous section) are scaled to the target spectral acceleration to perform dynamic analyses, and EDPs, such as ISDR, peak floor acceleration (PFA), peak floor velocity (PFV), and residual ISDR (RISDR), are obtained. (2) Assuming that the obtained EDPs are multivariate lognormal (Yang et al., 2009), a large number of additional EDPs are generated. Each realization of EDPs is a single Monte-Carlo simulation. (3) The damage states of structural and nonstructural components are estimated based on the simulated EDPs. (4) The seismic losses, including repair cost and repair time, of each component are determined based on its damage state and the FEMA P-58 database of componential seismic losses. (5) Component-level seismic losses are integrated into the seismic losses of the entire building.

A time-based loss assessment combines the intensity-based results and the SHC of the building, that is, mean annual frequency of exceedance (MAFE) of intensities. A series of seismic intensities, ranging from minor to major earthquakes, are considered. The seismic losses from different intensities are weighted by their probabilities of occurrence to calculate the MALs of the building.

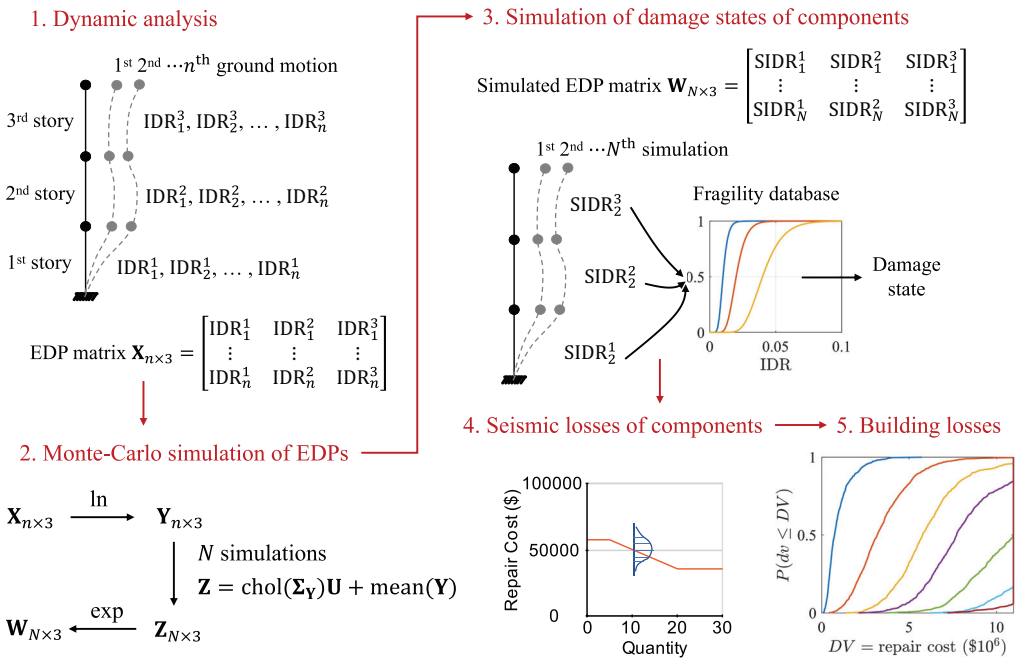

Figure 7. Flowchart of performing intensity-based loss assessment (adapted from FEMA P-58).

Structural components

Structural components vulnerable to earthquakes include BRB hold-downs, balloon-type CLT shear walls, and replaceable steel coupling beams. The fragility curves of these structural components are either available in FEMA P-58 database or derived from previous experiments in the literature (Ji et al., 2017, 2018; Shahnewaz et al., 2021).

All BRB hold-downs are located on the first floor. There are 8 BRB hold-downs in the X-direction and 12 in the Y-direction. Maximum axial strain is the EDP that determines the damage states of hold-downs. Fragility curves of BRB hold-downs are derived from those curves of commonly used BRB in FEMA P-58 database. The median ISDR of BRB corresponding to DS1 is 2% in FEMA P-58 (FEMA, 2018). Note that the commonly used BRBs are diagonal braces, but the BRB hold-downs are in vertical position. Assuming the angle between a common BRB and a horizontal line is equal to 45°, it can be derived that the ratio of ISDR to axial strain of a diagonal BRB is 1 to 2. This geometric relationship between ISDR and BRB axial strain is illustrated in Figure 8, assuming that deformations are infinitesimal and the axial strain of beams and columns are negligible. ISDR equals $\Delta l/l$ while BRB axial strain equals $\Delta l_b/l_b = \Delta l/2l$, which is half of ISDR. Then, 2% divided by 2 is regarded as the axial strain threshold of DS1 for BRB hold-downs. The fragility data of BRB hold-downs are summarized in Table 2.

There are 24 m^2 of CLT shear walls in the X-direction and 37.5 m^2 in the Y-direction for each story. Fragility curves are derived from the experiments (Shahnewaz et al., 2021) of balloon-type CLT shear walls. The average drift ratio of 2.7% that corresponds to the ultimate strength is considered as the EDP threshold of DS3; and 0.5% and 0.3% are the EDP thresholds of DS2 and DS1, respectively. For comparison, the EDP of DS3 of light

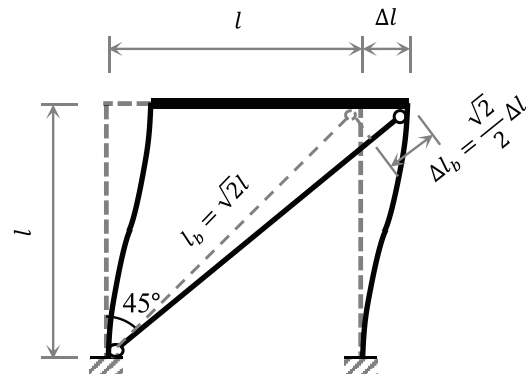

Figure 8. Geometric relationship between inter-story drift ratio and axial strain of a diagonal brace.

Table 2. Fragility of BRB hold-down

Damage state	EDP type	Median	Dispersion	Repair cost (US$ each)	Repair time (days)
DS1	Axial strain	1.0%	0.4	33,226–53,992	22–36

BRB: buckling restrained brace; EDP: engineering demand parameter; DS: damage state.

Table 3. Fragility of balloon-type CLT walls

Damage state	EDP type	Median (%)	Dispersion	Repair cost (US$ per 100 sq. ft)	Repair time (days per 100 sq. ft)
DS1	Story drift ratio	0.3	0.44	1840–2990	1.8–2.9
DS2		0.5	0.3	2337–3330	2.3–3.2
DS3		2.7	0.16	3825–5400	3.7–5.2

CLT: cross-laminated timber; EDP: engineering demand parameter; DS: damage state.

Table 4. Fragility of replaceable steel coupling beams

Damage state	EDP type	Median (%)	Dispersion	Repair cost (US$ each)	Repair time (days)
DS1	Link rotation angle	5	0.30	16,712–25,068	10–15
DS2		9	0.19	18,357–27,535	11.04–16.55
DS3		11	0.15	18,357–27,535	11.04–16.55

EDP: engineering demand parameter; DS: damage state.

framed wood walls in FEMA P-58 is 2.5%. DS3 of CLT shear walls indicates fracture of bolts or steel plates; DS2 indicates plastic deformation of steel joints; DS1 indicates that bolts come loose. Repair measures involve replacing the damaged joints or fastening the loose bolts. The fragility data of CLT walls are shown in Table 3.

There are two replaceable steel coupling beams in X-direction and four in Y-direction for each story. The rotation angle between two ends of a coupling beam is the EDP that determines its damage state. Fragility parameters of coupling beams are the same as those by Ji et al. (2017, 2018), listed in Table 4. DS3 indicates link fracture and the corresponding repair measure is to replace the damaged shear link; DS2 indicates link web of flange

Table 5. Quantity of nonstructural components

Pact fragility no.	Name	Performance group quantity	Unit	Dispersion	Direction	Floor
B2022.001	Curtain walls	58.61	30 SF	0.6	1	All
B2022.001	Curtain walls	58.61	30 SF	0.6	2	All
B3011.011	Concrete tile roof	37.51	100 SF	0.9	—	Roof
C1011.011a	Wall partition	14.06	100 LF	0.3	1	All
C1011.011a	Wall partition	14.06	100 LF	0.3	2	All
C2011.001a	Stairs	1.41	1 EA	0.1	1	All
C2011.001a	Stairs	1.41	1 EA	0.1	2	All
C3011.001a	Wall finishes	4.47	100 LF	0.4	1	All
C3011.001a	Wall finishes	4.47	100 LF	0.4	2	All
D2021.011a	Potable water piping	1.24	1000 LF	0.4	—	All
D3041.011a	HVAC ducting	0.58	1000 LF	0.6	—	All
D3041.031a	HVAC drops/diffusers	9.37	10 EA	0.4	—	All
D3041.041a	Variable air volume box	4.68	10 EA	0	—	All
D4011.021a	Fire sprinkler water piping	2.57	1000 LF	0.1	—	All
D4011.031a	Fire sprinkler drop	1.40	100 EA	0.1	—	All
D5011.011a	Transformer	11.70	1 EA	0.5	—	1
D5012.021a	Low voltage switchgear	0.04	225 AP	0.3	—	All
D5012.031a	Distribution panel	3.05	1 EA	0.2	—	1
D1014.011	Traction elevator	7.97	1 EA	0.8	—	1

EA: each; SF: square feet; LF: linear foot; HVAC: heating, ventilation, and air conditioning; AP: ampere.

buckling and repair measures include heating or replacing shear link; DS1 indicates slab damage.

Nonstructural components

FEMA P-58 Normative Quantity Estimation Tool is utilized to estimate the quantity of nonstructural components according to the building plan area and occupancy type. Occupancy types for all stories are apartment. The total quantity of each nonstructural component is listed in Table 5. Some components are directional, such as wall partitions and curtain walls, which means a single component of this type is only sensitive to vibration in either X- or Y-direction. Other components are nondirectional, which means their damage states depend on the maximum EDP in two directions.

Intensity-based loss assessment

The spectral accelerations corresponding to return periods of 475 and 2475 years are equal to 0.094 and 0.24g, respectively. Using the Python library PELICUN developed by SimCenter (Zsarnóczay and Zhong, 2020), intensity-based probabilistic seismic loss assessments are conducted for a series of different intensities ranging from 0.05 to 0.6g (0.25 to 2.5 times the 2475-year return period intensity). A total of 1000 Monte-Carlo simulations of EDPs are generated for each intensity. If the simulated maximum ISDR is larger than 5% (Teweldebrhan and Tesfamariam, 2022), the building is considered as collapse. The median RISDR threshold for being irreparable is 1% and dispersion is 0.3 (FEMA, 2018). If the building collapses or is irreparable due to large ISDRs or RISDRs, its repair cost is equal to reconstruction cost of the entire building and repair time is equal to reconstruction time. Otherwise, the building is repairable and its repair cost is calculated by accumulating the repair costs of all vulnerable structural and nonstructural components.

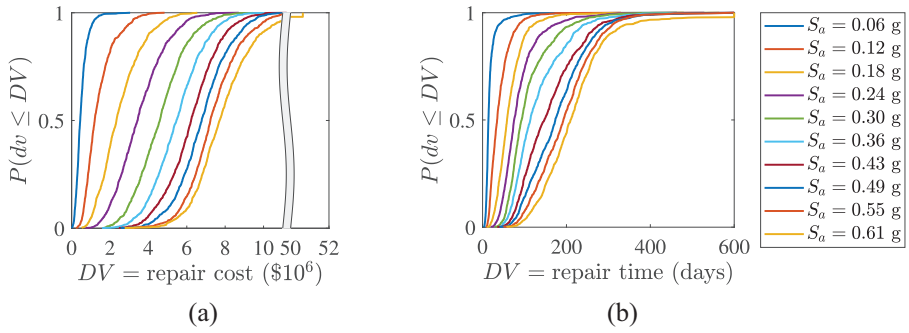

Figure 9. Cumulative distribution function of (a) repair cost and (b) repair time.

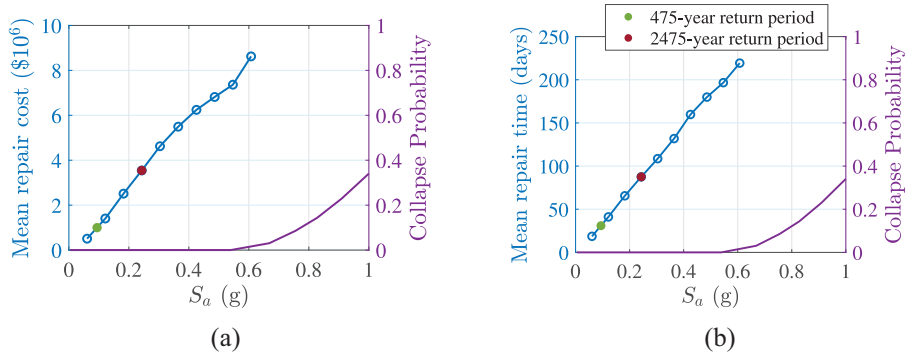

Figure 10. (a) Mean repair cost and (b) mean repair time with respect to spectral accelerations.

The reconstruction cost of the building is estimated to be US$216 per sq. ft (Sorathiya, 2019) and reconstruction time is 600 days. It is assumed that the maximum number of workers who are available for post-earthquake repairing is four on each floor. A parallel repair strategy is taken, which means repair on different floors can start simultaneously and the final repair time of the building depends on the longest one of all floors.

After performing intensity-based loss assessment, cumulative distribution functions (CDFs) of repair costs and repair times are shown in Figure 9 per level of spectral accelerations S_a. In Figure 9a, for the curves where S_a is higher than 0.6g, there is a sudden rise of CDF curve at the maximum repair cost (reconstruction cost). The sudden rise of CDF curve indicates a probability that repair cost is higher than reconstruction cost and thus a reconstruction strategy is preferred over a repairing strategy. For instance, when S_a is equal to 0.61g, the probability that the building will be reconstructed due to high repair cost is about 5%. Similarly, if the repair time is selected as the decision variable, the probability of reconstructing the building is 2% when S_a equals 0.61g, as shown in Figure 9b.

Mean repair cost and repair time with respect to spectral accelerations are presented in Figure 10. When S_a is smaller than 0.6g, most seismic losses are caused by damaged components, while contribution from collapse is negligible, because collapse probability is almost 0%. Under $S_a = 0.61$ g, mean repair cost is US$3.5 million, which is about 7% of the reconstruction cost; mean repair time is about 85 days. For all the examined intensities, repair cost is smaller than the reconstruction cost, and repair time is shorter than the reconstruction time, which implies that reconstruction hardly happens for this building.

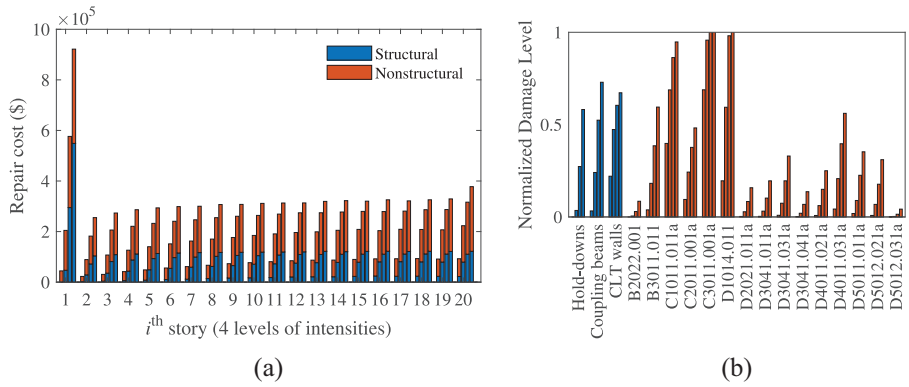

Figure 11. (a) Distribution of mean repair cost along elevation and (b) normalized damage levels (i.e. average damage states divided by the highest damage state) of different components. For each story/component, four seismic intensities (0.12, 0.24, 0.36, and 0.49*g*) are considered.

As the method utilized here is a component-level loss assessment, seismic losses from different components or stories can be readily obtained. Repair costs from different stories are shown in Figure 11a. For each story, there are four bars corresponding to four intensities of 0.12, 0.24, 0.36, and 0.49*g*. The first story has the highest repair cost because all hold-downs and some other nonstructural components (e.g. elevators and transformers) are located on the first floor. The 20th story has a relatively higher repair cost than other stories (except the first story) as some nonstructural components are only distributed on the roof. For other stories, repair costs rise with elevation, which is consistent with the trend of increasing deformation demand.

Damage levels of components, normalized by their maximum damage levels, are presented in Figure 11b. For example, the post-earthquake damage state of a component is DS2 and its highest possible damage state is DS3, then its normalized damage level would be $2/3 = 0.67$. It can be seen that hold-downs have almost no damage under a 2475-year return period earthquake ($S_a = 0.24$ *g*), while coupling beams and CLT walls have reached a 25% damage level. It implies that the coupling beams are the most important structural components that can contain vibration energy when intensities are smaller than the 2475-year return period intensity. At the intensity of 0.49*g*, the hold-downs reach a comparable damage level with that of the coupling beams and CLT walls.

Contributions to repair cost from different components are shown in Figure 12. Under a 475-year return period earthquake, nonstructural components contribute about 80% of total repair costs. With the increase of seismic intensities, contribution from structural components rises and reaches the peak at the intensity of $S_a = 0.4$ *g*. In particular, coupling beams contribute 80% to total repair costs of structural components under the 2475-year return period earthquake, and thus contribute more than any other type of components. As these steel coupling beams are replaceable, this CLT-CW building has a good replaceable property.

Time-based loss assessment

Time-based loss assessment is performed by combining intensity-based results and the SHC that is accessed online from *2020 National Building Code of Canada Seismic Hazard*

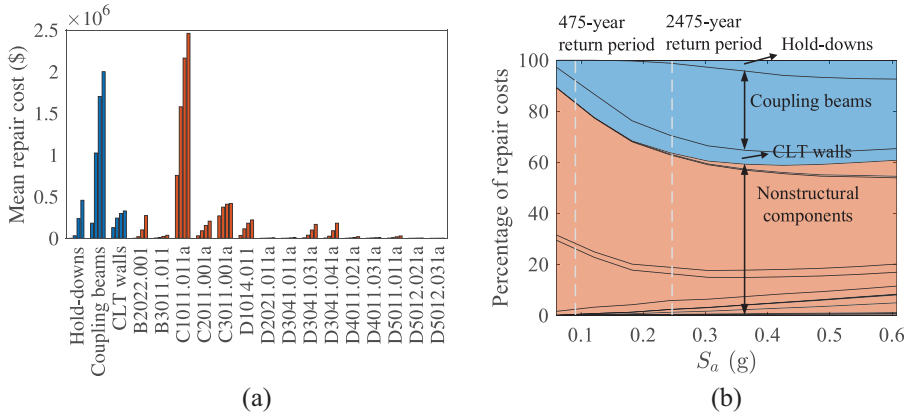

Figure 12. Mean repair costs of different components at given intensities. (a) Mean repair costs for seismic intensities of 0.12, 0.24, 0.36, and 0.49*g* and (b) percentage contribution of components.

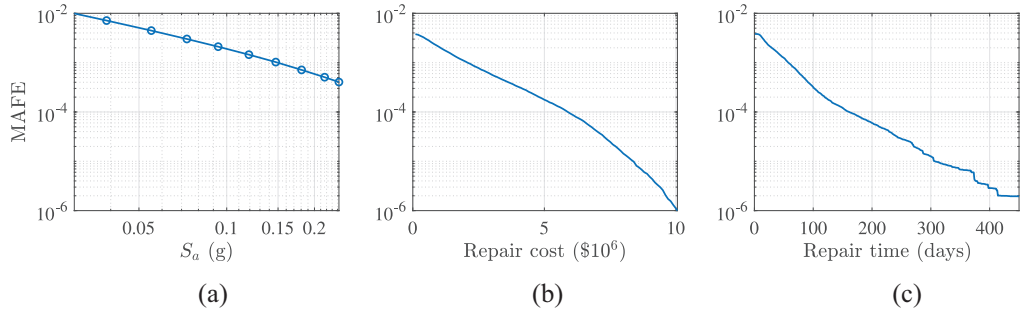

Figure 13. Mean annual frequency of exceedance of (a) spectral accelerations, (b) repair cost, and (c) repair time.

Tool (Natural Resources Canada, 2020). Building location is Vancouver and site class is C. The obtained SHC, that is, MAFE of spectral accelerations, is shown in Figure 13a.

The probability of exceedance of a certain seismic loss given an intensity $P(dv>DV|S_a)$ is complementary to CDF of the seismic loss $P(dv<DV|S_a)$ that has been obtained in Figure 9a. Combining $P(dv>DV|S_a)$ with SHC (denoted by $\lambda(S_a)$), MAFE of a certain loss is calculated as follows (Gunay and Mosalam, 2013; Mitrani-Reiser, 2007):

$$\lambda_{DV} = \int_{S_a=0.03}^{\infty} P(dv>DV|S_a)\mathrm{d}\lambda(S_a) \tag{1}$$

where DV denotes a type of decision variable (repair time or repair cost). Although the upper limit of integration is infinity, it does not mean numerous intensities should be examined. Actually, the contribution of a very high intensity is negligible due to its very small probability of occurrence. The maximum considered S_a here is 0.6*g*. Utilizing equation 1, λ_{DV} for repair cost and repair time are presented in Figure 13b and c, respectively.

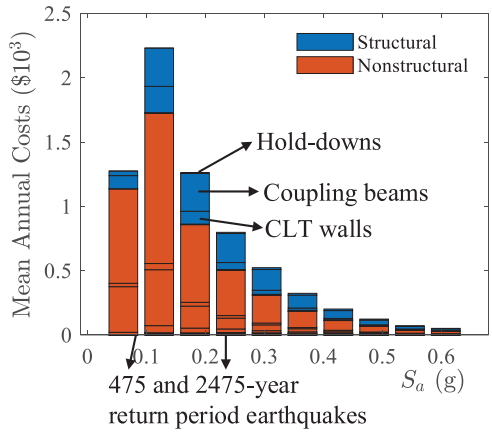

Figure 14. Mean annual repair costs from different intensities and components.

MAL is calculated as follows:

$$\mathrm{MAL} = \int_{S_a = 0.03}^{\infty} \overline{DV}(S_a)\mathrm{d}\lambda(S_a) \tag{2}$$

where $\overline{DV}(S_a)$ denotes the mean decision variables (repair time or repair cost) at a given intensity. Mean annual repair cost is estimated to be US$9000 and mean annual repair time is 0.28 days. Furthermore, these total losses can be broken down into losses from different intensities and components as shown in Figure 14. MAL peaks at 475-year return period intensities, which indicates that 475-year return period earthquakes have the greatest contribution to MAL. Earthquakes with lower intensities contribute less due to the less severe consequences. Although earthquakes with higher intensities can incur higher repair costs (shown in Figure 11a), the probability of occurrence of these higher intensities is relatively low. As a result, 475-year return period earthquake is the most important intensity level that affects the total MAL. Under most intensities (higher than 0.1g), the coupling beam is the component that contributes the most to the total structural repair cost, meaning that the coupling beam is the core structural component influencing the building seismic loss. Therefore, making these coupling beams replaceable is a reasonable and effective strategy to make CLT-CW building more resilient.

Seismic resilience assessment

While seismic loss is a measurement of the initial reduction of building function right after an earthquake, we can quantify seismic resilience of the building by examining the complete post-earthquake function recovery trajectory (Burton et al., 2018; Cimellaro et al., 2010). If the building function at a certain time after earthquake is denoted by $Q(t)$, the resilience index can be defined as (Bruneau et al., 2003; Cimellaro et al., 2010):

$$R = \int_{t=0}^{T_c} \overline{Q}(t)/T_c\mathrm{d}t \tag{3}$$

Table 6. Building interruption time multiplier (FEMA, 2020)

Structural damage state	Slight	Moderate	Extensive	Complete
Drift ratio (%)	0.5	1.5	2.5	5.0
Time multiplier	0	0.5	1.0	1.0

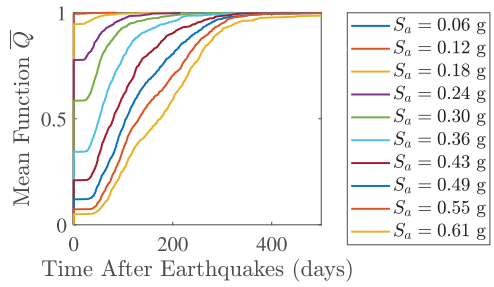

Figure 15. Mean function recovery trajectories after earthquakes.

where $\overline{Q}$ is the mean function; T_c is a control time to normalize the integral so that the resilience index $0 \leqslant R \leqslant 1$. Building function $Q(t)$ after an earthquake is not a deterministic function as there are uncertainties associated with earthquakes, structural responses, repair process, and so on. The mean function $\overline{Q}(t)$ can be estimated utilizing Monte-Carlo simulations. The closer to 1 the resilience index R is, the more resilient the building is.

As the building in this study is a residential apartment, it has a housing function. The function $Q(t)$ is equal to 1 if the building function has been restored, or else $Q(t) = 0$. The downtime of housing function (or function loss time) is a bit different from repair time that has been estimated in the last section. The building repair time is the time required to repair all damaged structural and nonstructural components. However, the building may recover to a normal function before all components have been completely repaired. For an apartment, its housing function has been restored as long as there is no danger for residents to live in. Therefore, the function loss time is often less than repair time. To estimate function loss time, repair time is multiplied by a multiplier that is less than or equal to 1 (FEMA, 2020). The multiplier, listed in Table 6, depends on structural damage state. For example, If the building is completely damaged, the multiplier is 1, which means function loss time is the same as repair time because both are equal to reconstruction time. If the building only has a slight damage, the multiplier is 0, which means a slight damage will not influence the housing function.

After conducting Monte-Carlo simulations, the mean recovery trajectories for different intensities are obtained, as shown in Figure 15. Although the recovery trajectory for a single simulation is a step function (because $Q(t)$ equals either 0 or 1), the mean function $\overline{Q}(t)$ is a smooth function. Mean function loss time, repair time, and resilience index corresponding to different intensities are listed in Table 7. The control time T_c for calculating resilience index is 500 days. Under the 2475-year return period intensity ($0.24g$), the mean function loss time is only 11.2 days, which demonstrates a good resilience. Function loss time at the same intensity of $0.24g$ is much smaller than repair time (86 days). For higher intensities, repair time and function loss time tend to approach an equal value.

Table 7. Seismic resilience indices under different intensities

Intensity (*g*)	0.06	0.12	0.18	0.24	0.30	0.36	0.43	0.49	0.55	0.61
Mean repair time (days)	17	43	66	86	109	133	160	180	195	219
Mean function loss (days)	0	0.1	3.6	11.2	31	60.3	92.2	120.8	146	177.4
Resilience	1	1	0.99	0.98	0.94	0.88	0.82	0.76	0.71	0.65

Conclusion

This study examines the probabilistic seismic performance and resilience of a 20-story CLT-CW building. A 3D nonlinear OpenSees model is developed to perform IDA using a set of bi-directional GM records that are selected to represent the seismicity of Vancouver, Canada. The probability distributions of economic losses and repair time at a series of spectral accelerations are presented by conducting intensity-based assessment. Mean annual losses and contribution from different components are also estimated to validate the repairability and seismic resilience of the building. The following conclusions can be drawn:

- The probability of being demolished due to unacceptable high repair cost is 0% under a 2475-year return period earthquake. The mean repair time and mean function loss time are 86 and 11.2 days, respectively, when a parallel repair strategy is taken.
- Except for the first and top story that have the highest repair costs, repair costs increase with rising elevation.
- The building has the highest mean annual loss under the 475-year return period intensity. Most repair costs are contributed from damaged components instead of building collapse.
- Steel coupling beams contribute about 80% to total repair costs of damaged structural components under 2475-year return period earthquakes, while the costs of hold-downs are small at the same intensity. Therefore, the coupling beam is the most important structural component that influences seismic losses of CLT-CW building, and further the replaceability of coupling beams makes the CLT-CW building resilient.

Nevertheless, some issues remain to be resolved in future research. (1) The plastic behavior and damage of steel joints within timber wall panels are not considered in FE modeling. (2) The seismic damage to water piping can cause water leak, which in turn may lead to additional repair costs of timber walls. (3) The floor diaphragms are assumed as rigid. Moreover, they are not explicitly modeled; rather, OpenSees' multi-point constraints feature is used to capture the desired behavior.

Declaration of conflicting interests

The author(s) declared no potential conflicts of interest with respect to the research, authorship, and/or publication of this article.

Funding

The author(s) disclosed receipt of the following financial support for the research, authorship, and/or publication of this article: This research was funded by the British Columbia Forestry Innovation

Investment's (FII) Wood First Program, the Natural Science Engineering Research Council of Canada Discovery Grant (RGPIN-2019-05013), and the Natural Science Foundation of China (NSFC) under Grant Nos 51820105013. The first author also wants to express his acknowledgment to the China Scholarship Council (CSC) for providing financial support to study at UBC Okanagan as a visiting student. Moreover, this research was supported in part through computational resources and services provided by Advanced Research Computing at the University of British Columbia.

ORCID iD

Tian You https://orcid.org/0000-0003-1671-2128

References

Almufti I and Willford M (2013) REDi™ rating system: Resilience-based earthquake design initiative for the next generation of buildings. Report, Arup Co, London.

American National Standards Institute (ANSI) (2012) *ANSI/APA PRG 320-2012 Standards for Performance-rated Cross-laminated Timber* (ANSI)/APA. Tacoma, WA: American National Standards Institute.

Baker JW (2011) Conditional mean spectrum: Tool for ground-motion selection. *Journal of Structural Engineering* 137(3): 322–331.

Breneman S and Richardson D (2019) Tall wood buildings and the 2021 IBC: Up to 18 stories of mass timber. *Woodworks*. Available at: https://www.woodworks.org/wp-content/uploads/wood_solution_paper-TALL-WOOD.pdf (accessed 19 September 2020).

Bruneau M and MacRae G (2017) Reconstructing Christchurch: A seismic shift in building structural systems. Report, Quake Center, University of Canterbury, Christchurch, New Zealand.

Bruneau M, Chang SE, Eguchi RT, Lee GC, O'Rourke TD, Reinhorn AM, Shinozuka M, Tierney K, Wallace WA and von Winterfeldt D (2003) A framework to quantitatively assess and enhance the seismic resilience of communities. *Earthquake Spectra* 19(4): 733–752.

Burton HV, Deierlein G, Lallemant D and Lin T (2016) Framework for incorporating probabilistic building performance in the assessment of community seismic resilience. *Journal of Structural Engineering* 142(8): C4015007.

Burton HV, Miles SB and Kang H (2018) Integrating performance-based engineering and urban simulation to model post-earthquake housing recovery. *Earthquake Spectra* 34(4): 1763–1785.

Canadian Standards Association (CSA) (2019) *Standard CSA 086-19: Engineering Design in Wood*. Mississauga, ON, Canada: Canadian Standards Association.

Chen Z and Popovski M (2020) Mechanics-based analytical models for balloon-type cross-laminated timber (CLT) shear walls under lateral loads. *Engineering Structures* 208: 109916.

Cimellaro GP, Reinhorn AM and Bruneau M (2010) Framework for analytical quantification of disaster resilience. *Engineering Structures* 32(11): 3639–3649.

Cook DT, Liel AB, Haselton CB and Koliou M (2022) A framework for operationalizing the assessment of post-earthquake functional recovery of buildings. *Earthquake Spectra* 38(3): 1972–2007.

Demirci C, Málaga-Chuquitaype C and Macorini L (2018) Seismic drift demands in multi-storey cross-laminated timber buildings. *Earthquake Engineering & Structural Dynamics* 47(4): 1014–1031.

Di Cesare A, Ponzo FC, Lamarucciola N and Nigro D (2020) Experimental seismic response of a resilient 3-storey post-tensioned timber framed building with dissipative braces. *Bulletin of Earthquake Engineering* 18(15): 6825–6848.

Fairhurst M, Zhang X and Tannert T (2014) Nonlinear dynamic analysis of a novel timber–steel hybrid system. In: *Proceedings of the world conference on timber engineering*. Available at: http://www.adivbois.org/wp-content/uploads/Can_0_Tech_Nonlinear-dynamic-analyses-of-novel-timber-steel-hybrid-system.pdf (accessed 17 January 2023).

FEMA (2006) Next-generation performance-based seismic design guidelines program plan for new and existing buildings. Report, Applied Technology Council (ATC). Redwood City, CA.
FEMA (2018) Seismic performance assessment of buildings. Report, Applied Technology Council (ATC). Redwood City, CA.
FEMA (2020) Hazus earthquake model technical manual. Report, FEMA, Washington, DC.
Furley J, van de Lindt JW, Pei S, Wichman S, Hasani H, Berman JW, Ryan K, Daniel Dolan J, Zimmerman RB and McDonnell E (2021) Time-to-functionality fragilities for performance assessment of buildings. *Journal of Structural Engineering* 147(12): 04021217.
Goda K and Atkinson GM (2011) Seismic performance of wood-frame houses in south-western British Columbia. *Earthquake Engineering & Structural Dynamics* 40(8): 903–924.
Guan X, Burton H and Moradi S (2018) Seismic performance of a self-centering steel moment frame building: From component-level modeling to economic loss assessment. *Journal of Constructional Steel Research* 150: 129–140.
Gunay S and Mosalam KM (2013) Peer performance-based earthquake engineering methodology, revisited. *Journal of Earthquake Engineering* 17(6): 829–858.
Halchuk S, Adams J and Allen T (2016) Fifth generation seismic hazard model for Canada: Crustal, in-slab, and interface hazard values for southwestern Canada. *Geological Survey of Canada Open File* 8090: 19.
Harte AM (2017) Mass timber–the emergence of a modern construction material. *Journal of Structural Integrity and Maintenance* 2(3): 121–132.
Ji X, Liu D and Molina Hutt C (2018) Seismic performance evaluation of a high-rise building with novel hybrid coupled walls. *Engineering Structures* 169: 216–225.
Ji X, Wang Y, Zhang J and Okazaki T (2017) Seismic behavior and fragility curves of replaceable steel coupling beams with slabs. *Engineering Structures* 150: 622–635.
Karacabeyli E and Gagnon S (2019) *Canadian CLT Handbook 2019 Edition*. Vancouver, BC, Canada: FPInnovations.
McKenna F, Fenves GL and Scott MH (2000) *Open System for Earthquake Engineering Simulation (OpenSees)*. Berkeley, CA: University of California, Berkeley. Available at: http://opensees.berkeley.edu (accessed 17 January 2022).
Medel-Vera C and Contreras MC (2021) Resilience-based predictive models for the seismic behaviour of mid-rise, base-isolated CLT buildings for social housing applications in Chile. *Journal of Building Engineering* 44: 103397.
Mieler M, Stojadinovic B, Budnitz R, Comerio M and Mahin S (2015) A framework for linking community-resilience goals to specific performance targets for the built environment. *Earthquake Spectra* 31(3): 1267–1283.
Milaj K, Sinha A, Miller TH and Tokarczyk JA (2017) Environmental utility of wood substitution in commercial buildings using life-cycle analysis. *Wood and Fiber Science* 49(3): 338–358.
Mitrani-Reiser J (2007) *An ounce of prevention: Probabilistic loss estimation for performance-based earthquake engineering*. PhD Thesis, California Institute of Technology, Pasadena, CA.
Moehle J and Deierlein GG (2004) A framework methodology for performance-based earthquake engineering. In: *13th world conference on earthquake engineering*, volume 679. WCEE Vancouver. Available at: https://www.iitk.ac.in/nicee/wcee/article/13_679.pdf (accessed 17 January 2023).
National Building Code of Canada (NBC) (2020) *National Building Code of Canada 2020* (NRCC). Ottawa, ON, Canada: National Research Council of Canada.
Natural Resources Canada (2020) 2020 national building code of Canada seismic hazard tool. Available at: https://www.seismescanada.rncan.gc.ca/hazard-alea/interpolat/nbc2020-cnb2020-en.php (accessed 1 December 2022)
Pei S, van de Lindt J, Barbosa AR, Berman J, Blomgren HE, Dolan J, McDonnell E, Zimmerman R, Fragiacomo M and Rammer D (2018) Full-scale shake table test of a two story mass-timber building with resilient rocking walls. In: *Proceedings, 16th European conference on earthquake engineering*. Thessaloniki, pp. 1–10. Available at: https://www.fpl.fs.usda.gov/documnts/pdf2018/fpl_2018_pei001.pdf (accessed 17 January 2023).
Pei S, van de Lindt J, Ricles J, Sause R, Berman J, Ryan K, Dolan J, Buchanan A, Robinson T, McDonnell E, Blomgren H, Popovski M and Rammer D (2017) Development and full-scale

validation of resilience-based seismic design of tall wood buildings: The Nehri Tallwood project. In: *Proceedings, 2017 NZSEE conference proceedings*, pp. 1–8. Wellington, NZ: New Zealand Society for Earthquake Engineering. Available at: http://db.nzsee.org.nz/2017/O5C.2_Ryan.pdf (accessed 17 January 2023).

Pei S, van de Lindt JW, Barbosa AR, Berman JW, McDonnell E, Daniel Dolan J, Blomgren HE, Zimmerman RB, Huang D and Wichman S (2019) Experimental seismic response of a resilient 2-story mass-timber building with post-tensioned rocking walls. *Journal of Structural Engineering* 145(11): 04019120.

Shahnewaz M, Dickof C and Tannert T (2021) Seismic behavior of balloon frame CLT shear walls with different ledgers. *Journal of Structural Engineering* 147(9): 04021137.

Smith SB and Coull A (1991) *Tall Building Structures: Analysis and Design*. London: John Wiley & Sons.

Sorathiya R (2019) *Literature review of cost information on mid-rise mass-timber building projects*. Report, SALA UBC, Vancouver, BC, Canada.

Structurlam (2021) *Structurlam Mass Timber Technical Guide for Cross Lam®clt and Glulamplus®, Canadian Version*. Structurlam Mass Timber Corporation, Intelligence in Wood. Available at: https://www.structurlam.com/wp-content/uploads/2021/10/Canadian_Technical_Guide_21.0_spreads.pdf (accessed 17 January 2022).

Svatoš-Ražnjević H, Orozco L and Menges A (2022) Advanced timber construction industry: A review of 350 multi-storey timber projects from 2000–2021. *Buildings* 12(4): 404.

Tesfamariam S (2022) Performance-based design of tall timber buildings under earthquake and wind multi-hazard loads: Past, present, and future. *Frontiers in Built Environment* 8: 848698.

Tesfamariam S and Goda K (2015) Seismic performance evaluation framework considering maximum and residual inter-story drift ratios: Application to non-code conforming reinforced concrete buildings in Victoria, BC, Canada. *Frontiers in Built Environment* 1: 18.

Tesfamariam S and Goda K (2022) Risk assessment of CLT-RC hybrid building: Consideration of earthquake types and aftershocks for Vancouver, British Columbia. *Soil Dynamics and Earthquake Engineering* 156: 107240.

Tesfamariam S, Skandalos K and Teweldebrhan BT (2021a) *Design of Tall Coupled-wall Timber Building: Energy Dissipating Coupling Beams*. Vancouver, BC, Canada: UBC Faculty Research and Publications.

Tesfamariam S, Skandalos K, Goda K, Bezabeh MA, Bitsuamlak G and Popovski M (2021b) Quantifying the ductility-related force modification factor for 10-Story timber–RC hybrid building using FEMA P695 procedure and considering the 2015 NBC seismic hazard. *Journal of Structural Engineering* 147(5): 04021052.

Teweldebrhan BT and Tesfamariam S (2022) Performance-based design of tall-coupled cross-laminated timber wall building. *Earthquake Engineering & Structural Dynamics* 51(7): 1677–1696.

Wilson AW, Phillips AR, Motter CJ, Lee JY and Dolan JD (2021) Seismic loss analysis of buildings with post-tensioned cross-laminated timber walls. *Earthquake Spectra* 37(1): 324–345.

Yang TY, Moehle J, Stojadinovic B and Der Kiureghian A (2009) Seismic performance evaluation of facilities: Methodology and implementation. *Journal of Structural Engineering* 135(10): 1146–1154.

Zsarnóczay A and Zhong K (2020) PELICUN. Available at: https://nheri-simcenter.github.io/pelicun (accessed 2 February 2022).